

OPEN

Effects of stacking periodicity on the electronic and optical properties of GaAs/AlAs superlattice: a first-principles study

M. Jiang¹, H. Y. Xiao^{1*}, S. M. Peng², L. Qiao¹, G. X. Yang², Z. J. Liu^{3*} & X. T. Zu¹

The effects of stacking periodicity on the electronic and optical properties of GaAs/AlAs superlattice have been explored by density functional theory calculations. Among the $(\text{GaAs})_m/(\text{AlAs})_m$, $(\text{GaAs})_1/(\text{AlAs})_m$ and $(\text{GaAs})_m/(\text{AlAs})_1$ ($m = 1$ to 5) superlattices, the band gaps of $(\text{GaAs})_m/(\text{AlAs})_1$ superlattices decrease significantly as the layer of GaAs increases, and the cut-off wavelengths are found to locate in the near infrared region. For $(\text{GaAs})_m/(\text{AlAs})_1$ SLs, the conduction bands shift toward Fermi level, resulting in the smaller band gap, while conduction bands of $(\text{GaAs})_1/(\text{AlAs})_n$ SLs slightly shift to higher energy, which lead to comparable band gaps. The layer number of GaAs shows negligible effects on the reflectivity spectra of superlattice structures, while the absorption coefficient shows a red-shift with the increasing layer of GaAs, which is beneficial for the application of GaAs/AlAs superlattice in the field of near infrared detector. These results demonstrate that controlling the number of GaAs layers is a good method to engineer the optoelectronic properties of GaAs/AlAs superlattice.

Recently, the novel artificial materials can be engineered on the molecular scale due to the development in the growth techniques (e.g. molecular beam epitaxy and metal-organic vapour phase epitaxy)¹. The semiconductor $(\text{GaAs})_m/(\text{AlAs})_n$ superlattices (SLs), in which m and n denote the number of stacking periodicity, have been widely applied in various optoelectronic devices, due to their unusual physical properties related to luminescence and optical absorption, etc²⁻⁷. Despite extensive studies on the electronic and optical properties of GaAs/AlAs SLs, such as band gap and absorption coefficient, there still lacks a comprehensive understanding of the effect of stacking periodicity on the optoelectronic properties of GaAs/AlAs SLs for its application as near infrared detector.

For the $(\text{GaAs})_1/(\text{AlAs})_1$ SL, which consists of one monolayer of GaAs and one monolayer of AlAs, its band gap at room temperature (RT) was determined to be 2.07 eV by an ellipsometry measurement⁸. The peak in resonant Raman scattering at RT has been reported to be at 2.006 eV by Kobayashi *et al.*⁹ and at 2.108 eV by Cardona *et al.*¹⁰. In the study of low-temperature photoluminescence of $(\text{GaAs})_1/(\text{AlAs})_1$ SL, Jiang *et al.* determined the band gap to be direct with the value of 2.214 eV¹¹. Isu *et al.* have used the photoluminescence measurement to investigate the ultrathin-monolayer $(\text{GaAs})_m/(\text{AlAs})_m$ ($m = 1\sim 4$) SLs and found that the luminescence peak locates at 2.033 eV for $(\text{GaAs})_3/(\text{AlAs})_3$ SL¹². Theoretically, Zhang *et al.* have studied the band structure for ultrathin $(\text{GaAs})_1/(\text{AlAs})_1$ SL employing first-principles method with a self-energy approach, and its band gap was direct with the value of 2.11 eV¹³. Ferhat *et al.* calculated the energy gap of $(\text{GaAs})_1/(\text{AlAs})_1$ SL employing the empirical pseudopotential method, which was reported to be 2.066 eV¹. Barkissy *et al.* studied the electronic structures of GaAs/AlAs SL at 4.2 K based on the envelope function formalism⁴. The direct band gap was found to be dependent on the temperature and decreased with the temperature increasing⁴. Botti *et al.* combined density functional theory (DFT) and semi-empirical method to study the band structures of $(\text{GaAs})_m/(\text{AlAs})_m$ SL, who found that for all sizes ($m \geq 1$) the band gap was direct³. Kahaly *et al.* used full-potential DFT method to investigate the epitaxial GaAs/AlAs SLs, and found the insulating characteristic of the interface¹⁴.

As for the optical properties of GaAs/AlAs SLs, Hidetoshi *et al.* investigated the optical absorption in a wide temperature range from 77 to 500 K, and a double-peak spectrum at 500 K was found¹⁵. Moore *et al.* investigated

¹School of Physics, University of Electronic Science and Technology of China, Chengdu, 610054, China. ²Institute of Nuclear Physics and Chemistry, Chinese Academy of Engineering Physics, Mianyang, 621900, China. ³Department of Physics, Lanzhou City University, Lanzhou, 730070, China. *email: hyxiao@uestc.edu.cn; lzjcaep@126.com

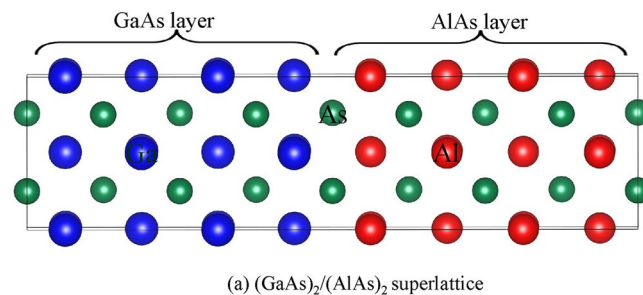


Figure 1. The geometry of (a) (GaAs)₂/(AlAs)₂ SL. The red, green and blue spheres are the Al, As and Ga atoms, respectively.

		Lattice constant (Å)	Band gap (eV)
GaAs	Our Cal.	5.63	0.50
	Other Cal.	5.60 ^a , 5.61 ^b	0.41 ^c
	Exp.	5.66 ^b	1.41 ^d
AlAs	Our Cal.	5.64	1.31
	Other Cal.	5.62 ^a , 5.63 ^b	1.35 ^c
	Exp.	5.62 ^b	2.23 ^d

Table 1. The lattice constant (Å) and band gap (eV) of bulk GaAs and AlAs. ^aRef. ³. ^bRef. ²⁰. ^cRef. ¹⁴. ^dRef. ²¹.

the photoluminescence of GaAs/AlAs SLs at low temperature and its band gap was found to be “pseudo-direct”¹⁶. Xia employed the tight-binding model to study the dielectric functions of GaAs/AlAs SLs, and found that the dielectric functions were different from those of bulk crystals, while they were similar to the average results of (GaAs)_m/(AlAs)_m ($m \geq 6$) SLs¹⁷. Tsu *et al.* measured the reflectivity of the GaAs/AlAs SL and reported that the absorption edge for the superlattice was approximately at 1.63 eV¹⁸. Lou *et al.* have used the macroscopic infrared dielectric tensor to analyze the reflectivity spectra of the GaAs/AlAs SL, and their results suggested that the superlattices resembled an anisotropic uniaxial crystal¹⁹.

In the literature, the researchers generally employed a standard DFT method, which underestimates the band gap of semiconductor SLs. In the present study, we employ a DFT method with reverse scissor correction to explore the optoelectronic properties of GaAs/AlAs SLs (see Fig. 1) in the field of near infrared detector. The results provide deep insights into the variation trend of optoelectronic properties with the stacking periodicity and may have important implications in tuning the electronic and optical properties of GaAs/AlAs SL.

Results and Discussion

The ground-state properties of bulk GaAs and AlAs. As shown in Table 1, the lattice constants of bulk AlAs and GaAs are calculated to be 5.64 and 5.63 Å, respectively, which agree well with the available results^{3,20}. As for GaAs/AlAs SL, the lattice constant is 5.635 Å, which may result from the negligible lattice mismatch between bulk states. The direct band gap of bulk GaAs is 0.5 eV and the indirect gap of bulk AlAs is 1.31 eV, which are comparable with other calculations¹⁴. The band gap of AlAs is found to be larger than that of GaAs, which is consistent with experimental results²¹.

The electronic properties of GaAs/AlAs superlattices. Based on the optimized structures, the band structures of (GaAs)_m/(AlAs)_n ($m, n = 1$ to 5) SLs are explored. Considering that the standard DFT method generally underestimates the band gap of materials^{22,23}, we calculated the band structure of bulk GaAs, bulk AlAs, and some representative superlattice structures employing DFT with scissor correction^{24–27} and hybrid DFT in the framework of Heyd-Scuseria-Emzefhof (HSE)²⁸. The approach of reverse scissor correction is an empirical correction consisting of a shift of the conduction regions up, which has been used to correct the band gap underestimated by DFT, especially to determine the band-gap offsets for interfaces between different semiconductors^{22,23,27,29}. The band gap for bulk GaAs, AlAs and (GaAs)_m/(AlAs)_m ($m = 1$ to 3) SLs obtained from DFT, DFT with scissor correction and hybrid DFT calculations are compared in Table 2. A scissor operator of 0.9 eV is employed, which corrects the band gap of GaAs from 0.5 to 1.40 eV and the band gap of AlAs from 1.31 to 2.21 eV, agreeing well with the experimental values of 1.41 eV and 2.23 eV²¹, respectively. The scissor operator of 0.9 eV is also applied to the (GaAs)_m/(AlAs)_m ($m = 1 \sim 3$) SLs. For (GaAs)₁/(AlAs)₁ SL, the corrected band gap of 2.04 eV is in excellent agreement with the experimental value of 2.07 eV⁸. Comparing the band gap obtained from DFT with scissor correction^{22,23,27,29} and hybrid DFT methods²⁸, we find that the results compare very well with each other. The DFT with scissor correction method, thus, is employed in the subsequent calculations.

The band gaps obtained from DFT with scissor correction for (GaAs)_m/(AlAs)_m ($m = 1$ to 5) SLs are presented in Table 3, as compared with the available theoretical results^{3,11}. The reverse scissor corrected band gaps of (GaAs)_m/(AlAs)_m SLs ($m = 1$ to 5) are shown to be direct. Botti *et al.* studied the electronic structures of GaAs/

	Band gap (eV)			
	DFT	DFT with scissor correction	Hybrid DFT	Exp.
GaAs	0.50	1.40	1.44	1.41 ^a
AlAs	1.31	2.21	2.16	2.23 ^a
(GaAs) ₁ /(AlAs) ₁	1.14	2.04	2.06	2.07 ^b
(GaAs) ₂ /(AlAs) ₂	1.08	1.98	1.99	—
(GaAs) ₃ /(AlAs) ₃	1.00	1.90	1.93	—

Table 2. A comparison of the band gap (eV) for bulk GaAs, AlAs and (GaAs)_m/(AlAs)_m (m = 1 to 3) SLs obtained from DFT, DFT with scissor correction and hybrid DFT calculations. ^aRef. ²¹. ^bRef. ⁸.

	(GaAs) _m					
	n	m				
		1	2	3	4	5
(AlAs) _n	1	2.04 (1.16 ^a , 2.07 ^b)	1.81	1.71	1.64	1.6
	2	2.15	1.98 (1.09 ^a)	1.84	1.75	1.69
	3	2.14	2.02	1.9 (1.02 ^a)	1.81	1.74
	4	2.13	2.01	1.94	1.84	1.76
	5	2.13	2	1.93	1.84	1.76

Table 3. The band gap (eV) for (GaAs)_m/(AlAs)_n (m, n = 1 to 5) SLs obtained from DFT with scissor correction. ^aRef. ³. ^bRef. ⁸.

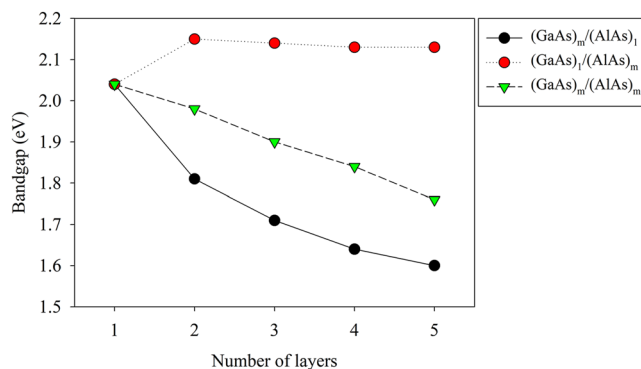


Figure 2. The band gap for (GaAs)_m/(AlAs)₁, (GaAs)_m/(AlAs)_m and (GaAs)_m/(AlAs)_m (m = 1 to 5) SLs obtained from DFT with scissor correction as a function of number of layers.

AlAs SLs employing DFT and semi-empirical method, and found that for all sizes ($m \geq 1$) the band gaps are direct at the Γ point³, which are consistent with our results. It is noted that the value of 1.98 eV for (GaAs)₂/(AlAs)₂ SL is slightly larger than the value of 1.76 eV for (GaAs)₅/(AlAs)₅ SL, indicating that the band gaps for (GaAs)_m/(AlAs)_m (m = 1 to 5) SLs decrease slowly as the stacking periodicity increases. Correspondingly, the cut-off wavelength of (GaAs)_m/(AlAs)_m (m = 1 to 5) SLs, $\lambda = 1240/E$, increases from 607 to 704 nm, which is located in the near infrared region.

We further analyze the band structures of (GaAs)_m/(AlAs)_n ($m \neq n$ and $m, n = 1$ to 5) SLs to investigate how the stacking periodicity affects their electronic properties (see Fig. 2). For the given layers of GaAs, the band gaps of SL structures are comparable with each other, and the cut-off wavelength of (GaAs)_m/(AlAs)_n SLs are all located near 607 nm. Besides, for the given layers of AlAs, the direct band gaps of SL structures decrease monotonously with the increasing layer number of GaAs. It is noted that the direct energy gap of 1.6 eV for (GaAs)₅/(AlAs)₁ SL is obviously smaller than the value of 2.04 eV for (GaAs)₁/(AlAs)₁ SL. The cut-off wavelength of (GaAs)_m/(AlAs)₁ (m = 1 to 5) SLs ranges from 607 to 775 nm. Furthermore, the direct band gap of (GaAs)₁₀/(AlAs)₁, (GaAs)₁₅/(AlAs)₁ and (GaAs)₂₀/(AlAs)₁ SLs obtained from the DFT with reverse scissor correction are determined to be 1.50, 1.46 and 1.44 eV, respectively, and the corresponding cut-off wavelength are calculated to be 826, 849 and 861 nm. These results indicate that controlling the layer number of GaAs is an effective way to tune the cut-off wavelength of GaAs/AlAs SLs in the field of near infrared detectors.

In order to explore the origin of the influences of the GaAs layer number on the electronic structure of GaAs/AlAs SLs, the density of state distribution (DOS) of (GaAs)₁/(AlAs)₁, (GaAs)₃/(AlAs)₁, (GaAs)₅/(AlAs)₁, (GaAs)₁/

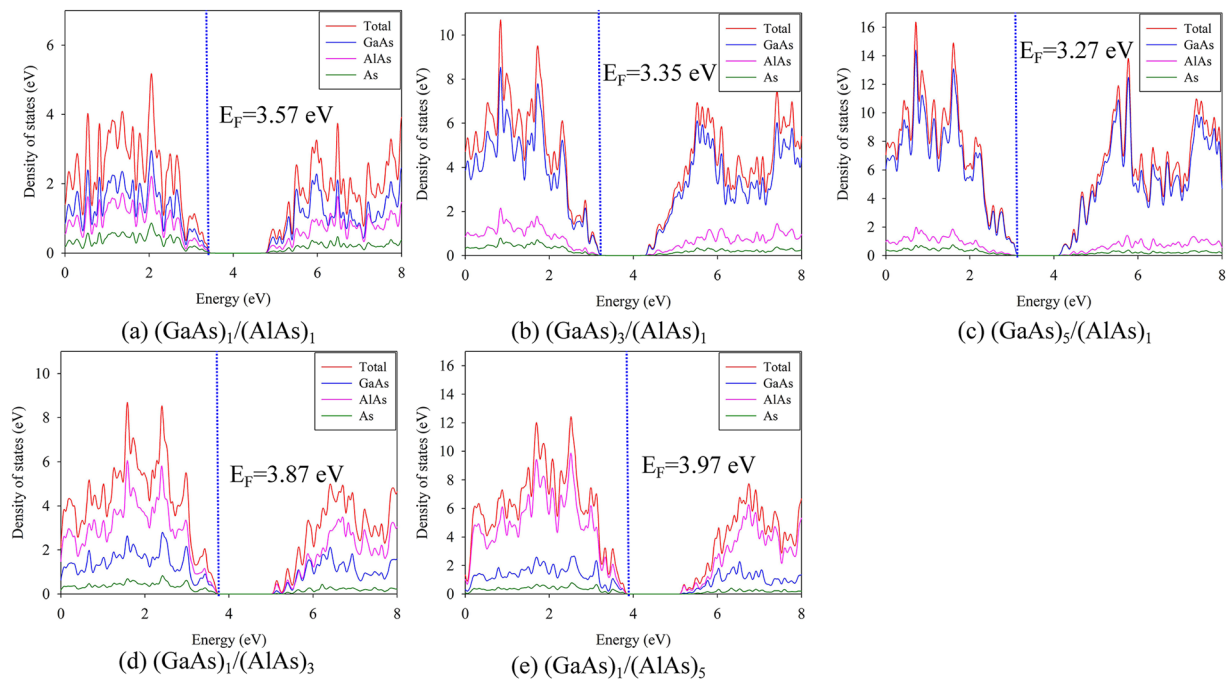


Figure 3. Atomic projected density of state distribution (DOS) for **(a)** $(\text{GaAs})_1/(\text{AlAs})_1$, **(b)** $(\text{GaAs})_3/(\text{AlAs})_1$, **(c)** $(\text{GaAs})_5/(\text{AlAs})_1$, **(d)** $(\text{GaAs})_1/(\text{AlAs})_3$ and **(e)** $(\text{GaAs})_1/(\text{AlAs})_5$ SLs. The Fermi level is indicated by the dashed line.

$(\text{AlAs})_3$ and $(\text{GaAs})_1/(\text{AlAs})_5$ SLs are analyzed and presented in Fig. 3. As compared with the DOS distribution of $(\text{GaAs})_1/(\text{AlAs})_1$ SL, the Fermi levels for $(\text{GaAs})_1/(\text{AlAs})_n$ and $(\text{GaAs})_m/(\text{AlAs})_1$ SLs shift to higher binding energy level and lower binding energy level, respectively. As for $(\text{GaAs})_m/(\text{AlAs})_1$ SLs, the valence bands are mainly contributed by GaAs (see Fig. 3(a~c)); in the case of $(\text{GaAs})_1/(\text{AlAs})_n$ SLs, the AlAs dominates the valence bands (see Fig. 3(a,d,e)). Also, the conduction bands of $(\text{GaAs})_1/(\text{AlAs})_n$ and $(\text{GaAs})_m/(\text{AlAs})_1$ SLs exhibit different character. For the $(\text{GaAs})_m/(\text{AlAs})_1$ SLs, the conduction bands shift toward the Fermi level, resulting in the smaller band gap, while the conduction bands of $(\text{GaAs})_1/(\text{AlAs})_n$ SLs shift slightly to higher energy, which lead to comparable band gaps. The different variation trend of the band gap of GaAs/AlAs SLs with the increasing layer of GaAs and AlAs, thus, is suggested to originate from their different electronic structures.

The optical properties of GaAs/AlAs superlattice. As stated above, controlling the layer of GaAs is a good method to tune the band gap and cut-off wavelength of GaAs/AlAs SLs. The effect of GaAs layer number on the absorption coefficient, reflectivity and electron energy loss spectrum of $(\text{GaAs})_m/(\text{AlAs})_1$ ($m = 1$ to 6) SLs are further investigated. The dielectric function is first calculated

$$\varepsilon(\omega) = \varepsilon_1(\omega) + i\varepsilon_2(\omega) \quad (1)$$

where $\varepsilon_1(\omega)$ and $\varepsilon_2(\omega)$ represent the real and imaginary parts, respectively, and ω is phonon energy³⁰. The $\varepsilon_2(\omega)$ is obtained from the momentum matrix elements between the valance and conduction wave functions³⁰, i.e.,

$$\varepsilon_2(\omega) = \frac{Ve^2}{2\pi\hbar m^2 \omega^2} \times \int d^3k \sum |\langle \varphi_c | p | \varphi_v \rangle|^2 \delta(E_c - E_v - \hbar\omega) \quad (2)$$

where φ_c and φ_v are the wave functions of the conduction and valence bands, respectively, p is the momentum operator, \hbar is the reduced Planck's constant, e is the electron charge, V is the unit cell volume. The $\varepsilon_1(\omega)$ is calculated by the Kramers-Kroenig relationship³⁰:

$$\varepsilon_1(\omega) = 1 + \frac{2}{\pi} M \int_0^\infty \frac{\varepsilon_2(\omega') \omega'}{\omega'^2 - \omega^2} d\omega' \quad (3)$$

where M represents the principal value of the integral. The absorption coefficient $\alpha(\omega)$, reflectivity $R(\omega)$ and electron energy loss function $L(\omega)$ are obtained from the $\varepsilon_1(\omega)$ and $\varepsilon_2(\omega)$ parts:

$$\alpha(\omega) = \sqrt{2} \omega \left[\frac{\sqrt{\varepsilon_1^2 - \varepsilon_2^2} - \varepsilon_1}{2} \right]^{\frac{1}{2}} \quad (4)$$

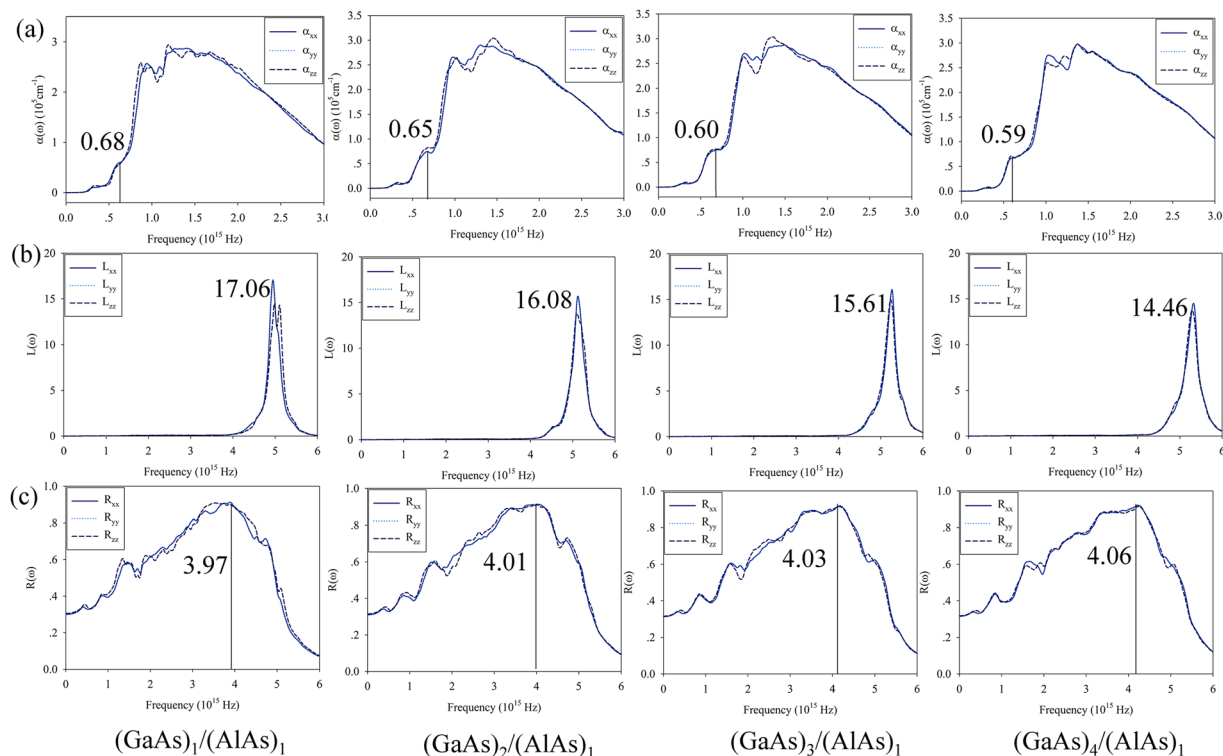


Figure 4. The (a) absorption spectra $\alpha(\omega)$, (b) electron energy loss spectra $L(\omega)$ and (c) reflectivity spectra $R(\omega)$ for $(\text{GaAs})_m/(\text{AlAs})_1$ ($m = 1$ to 4) SLs as a function of electromagnetic wave frequency.

$$R(\omega) = \frac{(n-1)^2 + k^2}{(n+1)^2 + k^2} \quad (5)$$

$$L(\omega) = \text{Im} \left\{ \frac{-1}{\varepsilon(\omega)} \right\}. \quad (6)$$

Figure 4 illustrates the optical properties of GaAs/AlAs SLs as a function of electromagnetic wave frequency. The absorption coefficient of GaAs/AlAs SLs is shown to be anisotropic, due to the reduction in symmetry (see Fig. 4(a)). The first peak of absorption spectra for $(\text{GaAs})_1/(\text{AlAs})_1$ SL appears at 0.68×10^{15} Hz. As the layer number of GaAs increases from 1 to 4, the first peak decreases gradually to 0.59×10^{15} Hz. Obviously, increasing the GaAs layer number causes a red shift of the absorption spectra for GaAs/AlAs SLs, which will benefit for their application as near infrared detector device. The properties about the elastically scattered and non-scattered electrons could be determined by the electron energy loss spectrum (EELS), and the results are illustrated in Fig. 4(b). The prominent peak of bulk GaAs is around 4.11×10^{15} Hz, which is comparable with the value of 4.04×10^{15} Hz reported by Ma *et al.*³¹. The peak of EELS for AlAs is located at $\sim 4.03 \times 10^{15}$ Hz. As shown in Fig. 4(b), the peaks of EELS for GaAs/AlAs SLs shift to lower energies and the peak intensity decreases significantly from 17.06 to 14.46 with the layer number of GaAs increasing. The reflectivity spectra of GaAs/AlAs SLs are further compared in Fig. 4(c). Similar to the absorption spectra and EELS, the reflectivity spectra for GaAs/AlAs SLs are anisotropic, as shown in Fig. 4(c). Clearly, the reflectivity shows a pronounced maximum at $\sim 4.0 \times 10^{15}$ Hz for all considered SLs. However, the layer number of GaAs has negligible effects on the reflectivity spectra of SL structures, and the spectra of all SLs are quite similar to each other. Lou *et al.* employed macroscopic infrared dielectric tensor to study the reflectivity of this SL structure, and found that the SL structures resemble an anisotropic uniaxial crystal¹⁹, which are consistent with our results. The results indicate that the layer number of GaAs has negligible effects on the reflectivity spectra of GaAs/AlAs SLs, while the absorption coefficient shows a red-shift with the increasing layer of GaAs. The presented study will advance the fundamental understanding of the optoelectronic properties of GaAs/AlAs superlattices for its application as near infrared detector.

Conclusions

In this study, the electronic and optical properties of GaAs/AlAs superlattices are explored by the density functional theory calculations with reverse scissor correction. The band gaps for $(\text{GaAs})_m/(\text{AlAs})_m$, $(\text{GaAs})_1/(\text{AlAs})_m$ and $(\text{GaAs})_m/(\text{AlAs})_1$ ($m = 1$ to 5) SLs are all direct. It is also noted that the reverse scissor corrected band gap of $(\text{GaAs})_m/(\text{AlAs})_1$ SLs decreases obviously with the increasing number of GaAs layer, and the corresponding cut-off wavelength all are located in the near infrared region. There is a red-shift for the absorption spectra of

(GaAs)_m/(AlAs)₁ superlattices with the layer of GaAs increasing, which is beneficial for their applications as near infrared detector. Besides, the maximum values of reflectivity of all SLs are much larger than those for bulk states. This study shows that the stacking periodicity of GaAs has remarkable effects on the electronic and optical properties of GaAs/AlAs SLs and varying the layer number of GaAs/AlAs SLs can be used to tune these properties effectively.

Methods

All the DFT calculations are implemented in Vienna *Ab Initio* Simulation Package (VASP)³². The ion-electron interactions are treated by the projector augmented-wave pseudopotentials^{33,34}, and the local-density approximation (LDA) in the form of Ceperly-Alder³⁵ is employed to describe the exchange-correlation functional. The convergence criteria for total energies and forces are 10⁻⁵ eV and 10⁻⁵ eV/Å, respectively. A cutoff energy of 500 eV and a 4 × 4 × 4 k-points are employed in these calculations. Three types of GaAs/AlAs SLs, i.e., (GaAs)_m/(AlAs)_m, (GaAs)₁/(AlAs)_m and (GaAs)_m/(AlAs)₁ (m = 1 to 5), are considered. Figure 1 illustrates the geometries of the representative (GaAs)₂/(AlAs)₂ SL.

Received: 20 August 2019; Accepted: 24 February 2020;

Published online: 17 March 2020

References

1. Ferhat, M., Zaoui, A. & Certier, M. Electronic structure calculation for (GaAs)(1)(AlAs)(1) monolayer superlattice. *Phys. Status Solidi B-Basic Res.* **204**, 673–678 (1997).
2. Botti, S. & Andreani, L. C. Electronic states and optical properties of GaAs/AlAs and GaAs/vacuum superlattices by the linear combination of bulk bands method. *Phys. Rev. B* **63**, 235313 (2001).
3. Botti, S., Vast, N., Reining, L., Olevano, V. & Andreani, L. C. Ab initio and semiempirical dielectric response of superlattices. *Phys. Rev. B* **70**, 045301 (2004).
4. Barkissy, D. *et al.* Electronic Properties of GaAs/AlAs Nanostructure Superlattice for Near Infrared Devices at Low Temperatures. *J. Low. Temp. Phys.* **182**, 185–191 (2016).
5. Barkissy, D. *et al.* Electronic transport and band structures of GaAs/AlAs nanostructures superlattices for near-infrared detection. *Appl. Phys. A-Mater. Sci. Process.* **123**, 0629 (2017).
6. Ribeiro, M., Fonseca, L. R. C. & Ferreira, L. G. First-principles calculation of the AlAs/GaAs interface band structure using a self-energy-corrected local density approximation. *Epl* **94**, 27001 (2011).
7. Spasov, S. *et al.* Modifying the electronic properties of GaAs/AlAs superlattices with low-density nitrogen doping. *J. Appl. Phys.* **100**, 2353793 (2006).
8. Alouani, M., Gopalan, S., Garriga, M. & Christensen, N. E. Interband Transitions in Ultrathin GaAs-AlAs Superlattices. *Phys. Rev. Lett.* **61**, 1643–1646 (1988).
9. Kobayashi, N., Toriyama, T. & Horikoshi, Y. Resonant Raman effect in thin-layered AlAs-GaAs superlattices. *Appl. Phys. Lett.* **50**, 1811–1813 (1987).
10. Cardona, M., Suemoto, T., Christensen, N. E., Isu, T. & Ploog, K. Electronic and vibronic structure of the (GaAs)1/(AlAs)1 superlattice. *Phys. Rev. B* **36**, 5906–5913 (1987).
11. Jiang, D. S., Kelting, K., Isu, T., Queisser, H. J. & Ploog, K. Luminescence properties of (GaAs)l(AlAs)m superlattices with (l,m) ranging from 1 to 73. *J. Appl. Phys.* **63**, 845–852 (1988).
12. Isu, T., Jiang, D. S. & Ploog, K. Ultrathin-layer (AlAs) m (GaAs) m superlattices with m = 1,2,3 grown by molecular beam epitaxy. *Appl. Phys. A* **43**, 75–79 (1987).
13. Zhang, S. B., Hybertsen, M. S., Cohen, M. L., Louie, S. G. & Tomanek, D. Quasiparticle band gaps for ultrathin GaAs/AlAs(001) superlattices. *Phys. Rev. Lett.* **63**, 1495–1498 (1989).
14. Kahaly, M. U., Nazir, S. & Schwingenschlogl, U. Band structure engineering and vacancy induced metallicity at the GaAs-AlAs interface. *Appl. Phys. Lett.* **99**, 3643049 (2011).
15. Hidetoshi, I., Hideki, K. & Hiroshi, O. Excitonic Absorption Spectra of GaAs-AlAs Superlattice at High Temperature. *Jpn. J. Appl. Phys.* **23**, L795 (1984).
16. Moore, K. J., Duggan, G., Dawson, P. & Foxon, C. T. Short-period GaAs-AlAs superlattices: Optical properties and electronic structure. *Phys. Rev. B* **38**, 5535–5542 (1988).
17. Xia, J. B. & Chang, Y. C. Electronic structures and optical properties of short-period GaAs/AlAs superlattices. *Phys. Rev. B* **42**, 1781–1790 (1990).
18. Tsu, R., Koma, A. & Esaki, L. Optical properties of semiconductor superlattice. *J. Appl. Phys.* **46**, 842–845 (1975).
19. Lou, B., Sudharsanan, R. & Perkowski, S. Anisotropy and infrared response of the GaAs-AlAs superlattice. *Phys. Rev. B* **38**, 2212–2214 (1988).
20. Ahmed, R., Hashemifar, S. J., Akbarzadeh, H., Ahmed, M. & Fazale, A. Ab initio study of structural and electronic properties of III-arsenide binary compounds. *Comput. Mater. Sci.* **39**, 580–586 (2007).
21. Monemar, B. Fundamental Energy Gaps of AlAs and AlP from Photoluminescence Excitation Spectra. *Phys. Rev. B* **8**, 5711–5718 (1973).
22. Lannoo, M., Schlüter, M. & Sham, L. J. Calculation of the Kohn-Sham potential and its discontinuity for a model-semiconductor. *Phys. Rev. B* **32**, 3890–3899 (1985).
23. Makinistian, L. & Albanesi, E. A. Ab initio calculations of the electronic and optical properties of germanium selenide. *J. Phys-Condens. Matt.* **19**, 186211 (2007).
24. Brik, M. G. First-principles study of the electronic and optical properties of CuXS₂(X = Al, Ga, In) and AgGaS₂ternary compounds. *J. Phys-Condens. Matt.* **21**, 485502 (2009).
25. O'Hara, A., Nunley, T. N., Posadas, A. B., Zollner, S. & Demkov, A. A. Electronic and optical properties of NbO₂. *J. Appl. Phys.* **116**, 213705 (2014).
26. Reshak, A. H., Auluck, S. & Kityk, I. V. Specific features in the band structure and linear and nonlinear optical susceptibilities of La₂CaB₁₀O₁₉. *Phys. Rev. B* **75**, 245120 (2007).
27. Zhang, S. *et al.* Band-Gap Reduction in BiCrO₃/BiFeO₃ Superlattices: Designing Low-Band-Gap Ferroelectrics. *Phys. Rev. Appl.* **10**, 044004 (2018).
28. Heyd, J., Scuseria, G. E. & Ernzerhof, M. Hybrid functionals based on a screened Coulomb potential. *J. Chem. Phys.* **118**, 8207–8215 (2003).
29. Mamoun, S., Merad, A. E. & Guilbert, L. Energy band gap and optical properties of lithium niobate from ab initio calculations. *Comput. Mater. Sci.* **79**, 125–131 (2013).
30. Kronig, R. & Kramers, H. Absorption and dispersion in x-ray spectra. *Z. Phys.* **48**, 174–179 (1928).

31. Ma, D. M., Chai, Y. Y., Wang, V., Li, E. L. & Shi, W. Electronic structure, magnetic and optical properties of Cr-doped GaAs using hybrid density functional. *Comput. Mater. Sci.* **113**, 75–79 (2016).
32. Kresse, G. & Hafner, J. Ab initio molecular dynamics for liquid metals. *Phys. Rev. B* **47**, 558–561 (1993).
33. Kresse, G. & Furthmüller, J. Efficient iterative schemes for ab initio total-energy calculations using a plane-wave basis set. *Phys. Rev. B* **54**, 11169–11186 (1996).
34. Kresse, G. & Furthmüller, J. Efficiency of ab-initio total energy calculations for metals and semiconductors using a plane-wave basis set. *Comput. Mater. Sci.* **6**, 15–50 (1996).
35. Ceperley, D. M. & Alder, B. J. Ground State of the Electron Gas by a Stochastic Method. *Phys. Rev. Lett.* **45**, 566–569 (1980).

Acknowledgements

H.Y. Xiao was supported by the NSAF Joint Foundation of China (Grant No. U1530129). Z. J. Liu was supported by National Natural Science Foundation of China (Grant No. 11464025) and the New Century Excellent Talents in University under Grant No. NECT-11-0906. The theoretical calculations were performed using the supercomputer resources at TianHe-1 located at National Supercomputer Center in Tianjin.

Author contributions

H.Y. Xiao and X.T. Zu designed the calculations. M. Jiang conducted the calculations and wrote the manuscript. S.M. Peng, G.X. Yang, Z. J. Liu and L. Qiao contributed the discussion and interpretation of the results. All authors discussed the results and reviewed the manuscript.

Competing interests

The authors declare no competing interests.

Additional information

Correspondence and requests for materials should be addressed to H.Y.X. or Z.J.L.

Reprints and permissions information is available at www.nature.com/reprints.

Publisher's note Springer Nature remains neutral with regard to jurisdictional claims in published maps and institutional affiliations.



Open Access This article is licensed under a Creative Commons Attribution 4.0 International License, which permits use, sharing, adaptation, distribution and reproduction in any medium or format, as long as you give appropriate credit to the original author(s) and the source, provide a link to the Creative Commons license, and indicate if changes were made. The images or other third party material in this article are included in the article's Creative Commons license, unless indicated otherwise in a credit line to the material. If material is not included in the article's Creative Commons license and your intended use is not permitted by statutory regulation or exceeds the permitted use, you will need to obtain permission directly from the copyright holder. To view a copy of this license, visit <http://creativecommons.org/licenses/by/4.0/>.

© The Author(s) 2020